http://dx.doi.org/10.14500/aro.12657

A Design of Power Amplifier using Enhanced Simple Real Frequency Technique

Alireza Golestanifar[1], Gholamreza Karimi[1†] and Ali Lalbakhsh[2]

[1]Department of Electrical Engineering, Faculty of Electrical and Computer Engineering, Razi University, Kermanshah, Iran

[2]School of Engineering, Macquarie University, Sydney, New South Wales, Australia

***Abstract*–In this paper, a novel discrete wide-band microstrip power amplifier (PA) is designed and fabricated based on the enhanced simple real frequency technique (ESRFT) to achieve a higher power added efficiency (PAE) over a wide frequency range compared to the conventional simple real frequency technique (SRFT). To compare the ESRFT with the SRFT, a basic PA using the SRFT is designed additionally. The ESRFT applies the feedback effects that play an important role in the PA design process, especially for high-frequency applications. Unlike the SRFT, the ESRFT considers both the back-end and the front-end impedance of the active device, while it is loaded by the designed input matching network (IMN) and the output matching network (OMN), respectively. The parasitic feedback elements of the transistor disturb the designed IMN and OMN. Therefore, an iterative method can converge to a better result. The matching networks (MNs) are modeled as a single matching problem, formulated and calculated in the Richard domain. The MNs are constructed by cascading microstrip unit elements (UEs) to obtain a wide-band simple structure. The characteristic impedances of the UEs are derived using the Richard extraction process. The fabricated PA shows good agreement between the simulation and measurement results. It has a wide-band gain of up to 13 dB from 0.8 GHz to 1.6 GHz, with a maximum PAE of about 70% that has been improved compared to the designed basic PA. Furthermore, the third harmonic is suppressed up to 25 dBc.**

***Index Terms*—Matching network, Microstrip, Power added efficiency, Power amplifier, Real frequency technique.**

I. Introduction

To design a wide-band power amplifier (PA) and Doherty PA, microstrip filters and couplers are very applicable. Artificial neural networks can model and calculate a proper model to design a wide-band microstrip coupler (Roshani, et al., 2025; Mohamadpour, Karimi, and Roshani, 2025). Wide-band microstrip filters are another component used in the design of wide-band PAs (Roshani, et al., 2024). Wide-band equalizers, filters, and matching networks (MNs) are the essential components of modern communication systems. The main task of wide-band MNs is to transfer as much power as possible with a flat gain over a wide frequency span (Yarman, 2008), whereas the amount of power to be transferred is limited by the frequency bandwidth and the immittance divergence between the load and the generator. To transfer a wide-band signal to a load, such as a 50 Ω antenna, wide-band MNs are required. From a technical point of view, a matching problem consists of the following four important concepts:

1. Active matching problem, creating a matching between two active devices
2. Insertion loss or filter problem, creating matching between a resistive load and a generator
3. Single matching problem, creating a matching between a complex load and a resistive generator
4. Double matching problem, creating a matching between the complex generator and the complex load.

The design process for a wide-band MN is mostly based on passive and lossless elements. As a result, important topics of Darlington's theorem, positive real function, bounded realness, Foster function, and Belevitch form have been raised (Yarman, 2010; Youla, 1964). There are three main design methods for wide-band MNs. The first is the analytical method, in which analytical theories are used to gain bandwidth limits; however, it is mostly effective for simple matching problems with one or two reactive elements. It also requires a circuit model of the load to be matched, as explained in (Youla, 1964). The second option is to use professional computer-aided design software and its optimization facilities. An MN circuit topology is necessary for circuit design and optimization. Furthermore, a good initialization of the parameter values for the optimization process is important for result convergence (Jia, et al., 2018). Real frequency technique (RFT) is the third method that can be used for both the optimization process and analysis. The RFT does not necessarily need an equalizer. It converges the objective function to a proper answer. The RFT uses

ARO-The Scientific Journal of Koya University
Vol. XIV, No.1 (2026), Article ID: ARO.12657. 8 pages
DOI: 10.14500/aro.12657
Received: 01 October 2025; Accepted: 26 February 2026
Regular research paper; Published: 10 April 2026
†Corresponding author's e-mail: ghkarimi@razi.ac.ir

real frequency (RF) values, such as scattering or immittance values for different frequency points (Carlin, 1977). Line segment RFT (LSRFT) uses only piecewise linear function estimation of the equalizer, and then its imaginary part is derived using a Hilbert transform. However, the LSRFT is limited to single matching problems. Direct Computational RFT (DCRFT) uses the immittance parameters as the driving point function (DPF) of a load and a generator to obtain a proper MN (Yang, et al., 2018). This method is suitable for low-frequency MNs and has more non-linear equations for the optimization process compared to the simple real frequency technique (SRFT). The SRFT uses scattering parameters and equations that are applicable to microwave design (Tran, Henderson and Gengler, 2019); (Kouhalvandi, Ceylan and Ozoguz, 2020). A smart wide-band C-band discrete microstrip PA with high drain efficiency was designed and fabricated using the SRFT, radial stubs, and a harmonic control network. The microstrip MNs and the novel formulas are derived to match different impedance values over various frequency bands. Coupled microstrip lines are applied to create a wide stop-band, and the SRFT is used to design an MN in (Golestanifar and Karimi, 2021). The SRFT has been applied to create the fundamental MNs. In (Krauss, Bostian and Raab, 1991), a new method to assess the gain limitations is introduced. Furthermore, it declares whether the MN via obtained load-pull values are realizable or not.

The RFT bypasses the conventional design techniques, such as creating and finding a proper circuit model and then solving too many differential equations. SRFT is one of the best matching design methods, and it is famous for its easy design process, which will converge to a proper answer in a short time. The enhanced SRFT (ESRFT) is more complex than SRFT because it is more complete. It will consider feedback effects to converge on a better answer. Conventional SRFT is applicable to design wide-band MNs for an amplifier whose active device is almost unilateral, but at high frequency and high-power applications, parasitic elements show their influence on the device and make it more non-linear and bilateral. Therefore, it is essential to have a smaller active device with a higher power capacity. Larger dimensions mean more parasitic effects. The contribution of this paper is a novel idea to present an approach to design wide-band MNs for a radio frequency PA, taking parasitic feedback effects into account to achieve high output power and better MNs. In this paper, first, the single matching problem is explained, and then a PA is designed using conventional SRFT. Then the ESRFT is explained, and it is mentioned how it improves both input and output MNs synchronously. Unlike the conventional SRFT, which treats the input and the output MNs as two independent single-matching problems under the quasi-unilateral device assumption, the proposed ESRFT formulates the PA design as a coupled double-matching problem in the presence of parasitic feedback ($S_{12}\neq 0$). In ESRFT, the IMN and OMN are redesigned iteratively while considering their mutual influence on the front-end and back-end reflection coefficients of the active device. This transforms the matching task from two independent problems into a coupled optimization problem in the RF domain, which constitutes the main theoretical contribution of this work.

II. Single Matching Problem

The single matching problem is considered to design MNs for the microwave PA, as in most practical cases, the load and the generator have a fixed load value of 50Ω. Furthermore, the input and the output of an active device have different impedance values over its frequency bandwidth. Fig. 1 shows Fano's model for the single matching problem.

A complex impedance over a frequency bandwidth is modeled by a two-port network [L] and a pure resistive load (Darlington's theorem), and [E] is a two-port equalizer. The parameters of [E] are to be found during the optimization process via an objective function.

III. Richard Domain

Neither lumped capacitors nor lumped inductors operate correctly in the microwave band. Therefore, the microstrip transmission line can be used for designing microwave discrete circuits. The input reflection coefficient (S_{in}) of a lossless microstrip line terminated in a load (Z_L) is:

$$Sin = (1-j\ tan(\beta l))/(1+tan\ (\beta l))\ S_L \quad (1)$$

Where S_L is the reflection coefficient at the load, and β is the pure imaginary propagation coefficient, and L is the physical length of the microstrip line. Richard's variable for the lossless line is explained as:

$$\lambda = j\ tan\ (\beta l) \quad (2)$$

Therefore:

$$S_{in} = ([1-\lambda]/[1+\lambda]\ S_L) \quad (3)$$

Equation (4) shows the rational form of a lossless two-port circuit constructed with microstrip commensurate lines.

$$[S] = \begin{bmatrix} \frac{h(\lambda)}{g(\lambda)} & \frac{f(\lambda)}{g(\lambda)} \\ \frac{f(\lambda)}{g(\lambda)} & (-1)^{q+1}\frac{h(-\lambda)}{g(\lambda)} \end{bmatrix} \quad (4)$$

Where:

$$f(\lambda) = \lambda^q \prod_{l=1}^{n_z} (\lambda^2 + \Omega_l^2)(1-\lambda^2)^{\frac{k}{2}} \quad (5)$$

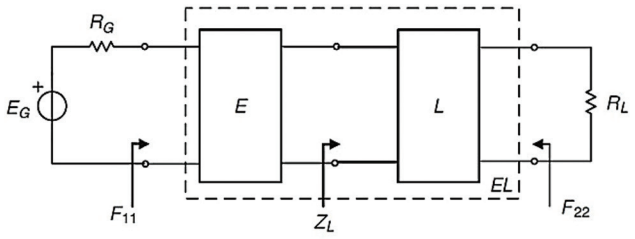

Fig. 1. Fano's model for the single matching problem.

 http://dx.doi.org/10.14500/aro.12657

Moreover, S is a bounded real matrix. The $g(\lambda)$ is a strictly Hurwitz polynomial, and the $h(\lambda)$ is a Hurwitz polynomial. The k is the total number of the cascaded UEs, and the q is the number of transmission zeros at DC. The n_z is the total number of the finite zeros of the $j\Omega$ axis.

Transmission zeros can determine a circuit topology. The transducer power gain (TPG) of a lossless two-port is:

$$TPG = f(\lambda)f(-\lambda)/g(\lambda)g(-\lambda) = F(\lambda)^2/G(\lambda)^2 \quad (6)$$

In a lossless two-port MN, the roots of the $g(\lambda)$ must construct a Hurwitz polynomial (Yarman, 2010) strictly. The Richard extraction method is used to design MNs of a PA. A UE is a microstrip transmission line with a constant physical length of $\lambda/4$, where λ is the wavelength at the last RF value at the stop-band. Commensurate lines are UEs with different positions (cascaded, shunt, or series open or short stubs) used to construct a microstrip circuit. Fig. 2 shows commensurate lines and their various possible positions, such as series stubs, open-ended and short stubs, where series stubs are applied in this paper.

The design process of microwave circuits through commensurate lines is an analytical and proven approach in communication system circuits. Kurada identities can be applied to change the topology options of commensurate lines. These identities replace capacitive loading with inductive loading and vice versa. In this design, only cascaded UEs are used. Richard's extraction is applied to design a circuit with a cascade connection of UEs with different characteristic impedances. A MATLAB program is able to analyse it. Fig. 3 shows Richard's extraction conceptual model.

This method extracts the characteristic impedance of each cascaded UE by altering the normalized characteristic impedance of the circuit's reflection coefficient for each section. Richard's extraction procedure and its equations are explained in (Yarman, 2008).

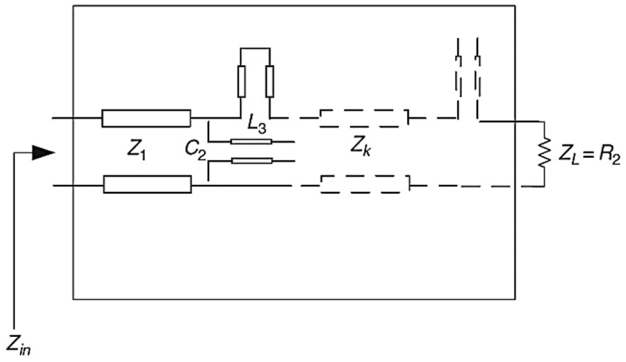

Fig. 2. Commensurate lines and their various possible positions.

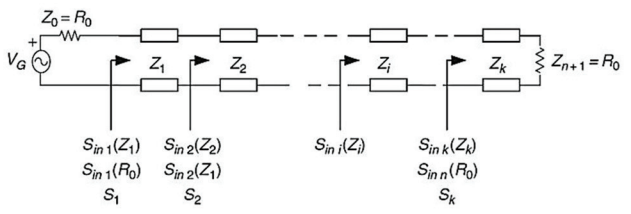

Fig. 3. Richard extraction conceptual model.

IV. Gain and matching equations

Fig. 4 shows the PA design model and the active device parameters, such as scattering parameters and reflection coefficients. The IMN, the OMN, the front-end, and the back-end reflection coefficients are Γ_S, Γ_L, Γ_{in}, and Γ_{out}, respectively.

To transfer maximum power from the IMN to the front end of the active device, the following equation should be satisfied:

$$\Gamma_{in} = \Gamma_s^* \quad (7)$$

$$\Gamma_{in} = S_{11} + \frac{S_{12}S_{21}\Gamma_L}{1 - S_{22}\Gamma_L} \quad (8)$$

Moreover, to transfer maximum power from the back-end of the active device to the OMN, the following equation should be satisfied:

$$\Gamma_{out} = \Gamma_L^* \quad (9)$$

$$\Gamma_{out} = S_{22} + \frac{S_{12}S_{21}\Gamma_s}{1 - S_{11}\Gamma_s} \quad (10)$$

Therefore, to have maximum gain and least dissipation power, both (7) and (9) should be satisfied, and if $S_{12} \neq 0$, then Γ_{out} is affected by Γ_{in} and vice versa. It means that when the IMN is designed, the OMN will be affected by it and should be redesigned at the same time. When the OMN is designed, the IMN is affected and should be redesigned. This process can continue to converge to a good answer. Therefore, the feedback effect ($S_{12} \neq 0$) needs to be considered in the design process. Here, the ESRFT will be applicable.

Fig. 5 shows a small signal model of an HEMT. Some elements that are making feedback effects are highlighted in the red boxes, including the transistor source parasitic resistor and the inductor that are created by the package leads and the intrinsic gate to drain capacitance.

V. Design and Fabrication using SRFT

To declare and to compare the ESRFT with the conventional SRFT, a basic PA using SRFT was designed and simulated. The PA has 6 UEs in the IMN and 5 UEs in the OMN. In microwave and RF devices, it is hard to measure immittance parameters. SRFT uses neither impedance

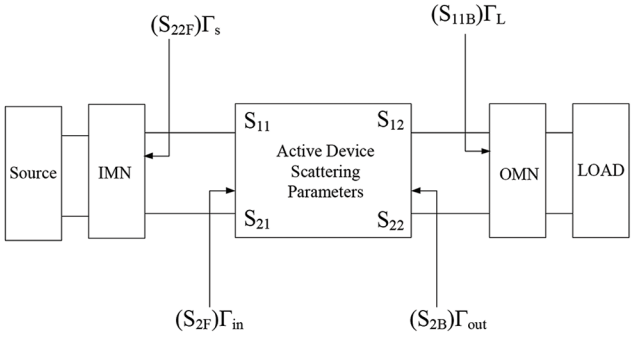

Fig. 4. Power amplifier design model.

nor admittance, but instead, it directly specifies scattering parameters derived simply by measurement or simulation. The optimization process can be easily applied to equations that are derived according to S parameters. LSRFT and DCRFT use DPFs that are defined by immittance parameters. As a result, SRFT is more straightforward and faster than other conventional RFTs. An effective conventional process to design a wide-band microstrip amplifier using SRFT was presented in (Yarman, 2010). Fig. 6a shows the first step, and Fig. 6b the second step design by conventional SRFT.

First, to design the PA, an IMN at the front end of the PA is designed, while there is typically a 50 Ω resistive load at the output of the active device. The second step is to design the OMN while considering the designed IMN applied to the front end of the device. The back-end reflection coefficient is considered to design the OMN as follows:

$$S_{2B} = S_{22} + (S_{12}\, S_{21})/(1\text{-}S_{11}\, S_{22F}) \quad (11)$$

In this case, the IMN affects the back-end reflection coefficient. S_{22F} is the IMN reflection coefficient that has been designed in the first step. In the conventional method, S_{11}, S_{12}, S_{21}, and S_{22} are scattering parameters of the biased device, and these parameters are only suitable for linear operation. The proposed PA operates in a non-linear mode. Therefore, the output impedance is non-linear. To apply non-linear effects, load-pull simulation results for maximum PAE and gain or power are applied as shown in Fig. 7, and the S_{22} values are replaced here by the non-linear amounts. To make the active device more stable, a parallel RC circuit was added and tuned at the input port of the active device, R= 36 Ω and C= 6 pF. The S_{22} is:

$$S_{22} = (Z_{out} - Z_0)/(Z_{out} + Z_0) \quad (12)$$

The same process is applied for the S_{11} as follows:

$$S_{11} = (Z_{in} - Z_0)/(Z_{in} + Z_0) \quad (13)$$

The RF data applied for SRFT and even ESRFT start from 0.8 GHz, and there is no DC or finite transmission zero; therefore, it is easy to use Richard extraction for PA design, so only cascaded UEs are applied. Furthermore, the biased active device has been tuned to be stable. As a result, any desired MN is applicable without creating any unstable conditions. Fig. 8a shows the scattering parameters, and the maximum available gain (MAG) of the under-biased device, and Fig. 8b shows the K-factor or stabfact and the M-factor or stabmeas values. It is seen that the device is stable, and the S_{11} shows that there is no good matching at the input port, and the S_{22} shows that there is already a good matching at the output port, especially at lower frequencies, compared to the input port. Furthermore, S_{12} shows that the feedback effects will increase with the frequency.

Fig. 9a shows the gain and the PAE simulation results, and Fig. 9b shows the fundamental and the third harmonic simulation results for an input power of 16 dBm, and Fig. 9c shows the S_{11} and S_{22} parameters. As can be seen, the gain ranges from 11.3 dB to 12.3 dB. Furthermore, the PAE result is not very satisfying, between 41% and 54%. It is seen that they have been improved by SRFT, but it is not as satisfying compared to ESRFT, whose scattering parameters will be shown.

VI. ESRFT

Due to the parasitic elements of an active device, it is not unilateral (Krauss, Bostian and Raab, 1991). Especially, devices operating at high frequency and high power will have drastic feedback effects. In the conventional SRFT process,

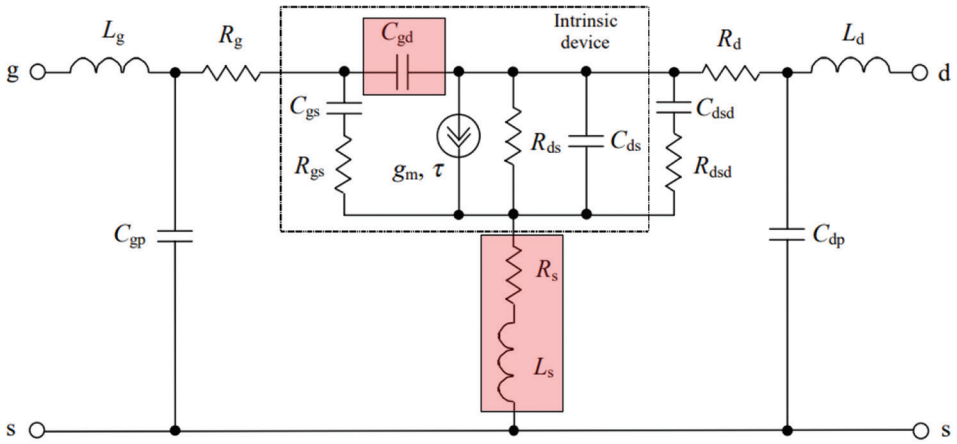

Fig. 5. Small signal model of HEMT transistor.

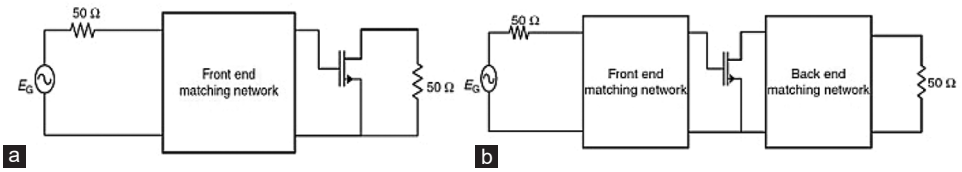

Fig. 6. Design steps using conventional simple real frequency technique: (a) first step, (b) second step.

http://dx.doi.org/10.14500/aro.12657

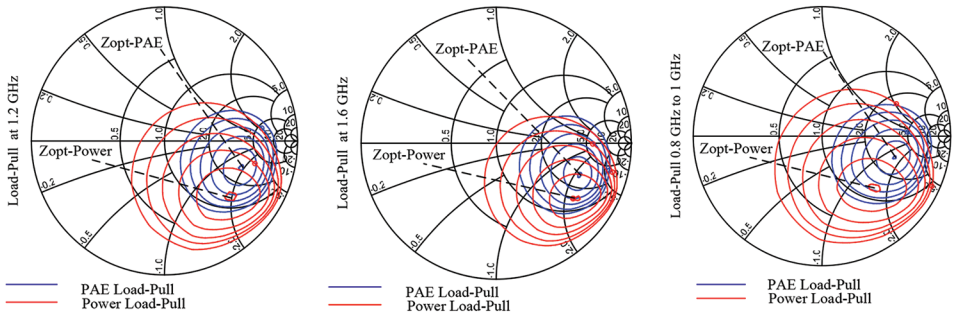

Fig. 7. Load-pull simulations for an input power of 16 dBm.

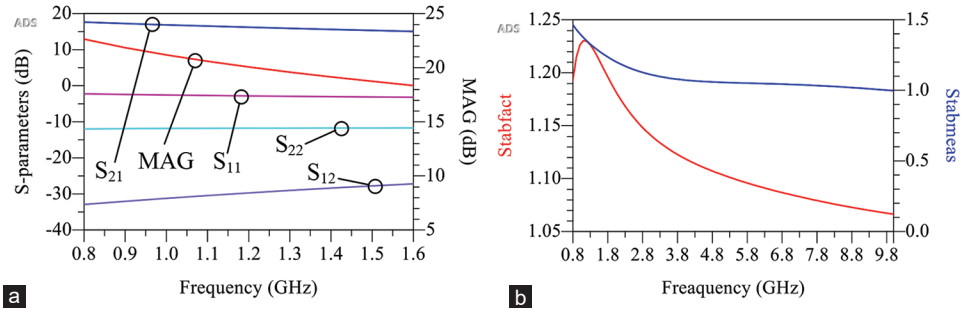

Fig. 8. (a) Scattering parameters and maximum available gain, (b) K-factor and M-factor values.

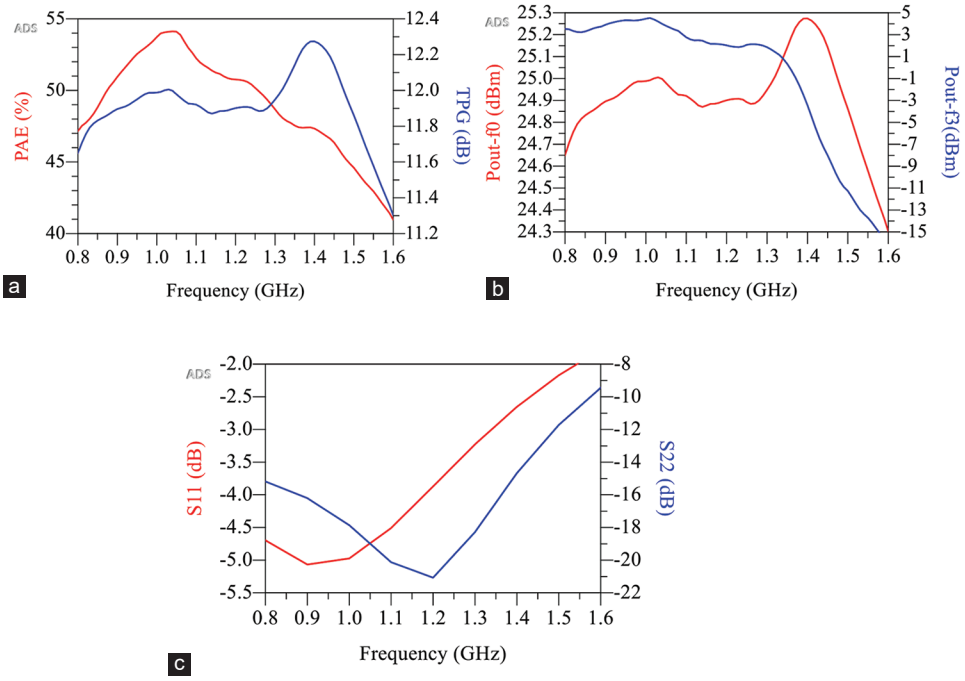

Fig. 9. Basic power amplifier characteristics: (a) power added efficiency and transducer power gain, (b) fundamental and third harmonic output power, (c) S_{11} and S_{22} parameters.

only the effects of the designed IMN have been considered to design the OMN. The idea is to redesign the IMN while it is connected to the designed OMN. The design process will be optimized by affecting both the front-end and the back-end reflection coefficients. A PA using the idea was designed and simulated according to ESRFT.

The main difference between SRFT and ESRFT can be summarized as follows:

1. SRFT assumes quasi-unilateral behavior (S_{12}=0) or only considers it once when the IMN is designed, whereas ESRFT considers bilateral behavior (S_{12}≠0)
2. SRFT designs IMN and OMN sequentially; ESRFT designs them interactively
3. SRFT solves two independent single-matching problems, whereas ESRFT solves a coupled double-matching problem

4. ESRFT updates both the front-end and back-end reflection coefficients during the design process
5. ESRFT leads to improved matching quality and higher PAE by accounting for feedback effects.

Equation (18) explains the front-end reflection coefficient.

$$S_{2F}=S_{11}+ (S_{12}S_{21})/(1-S_{22}S_{11B}) \quad (14)$$

Where S_{11B} is the input reflection coefficient of the designed OMN. The convergence of ESRFT iterations is defined when the variation of both the front-end and back-end reflection coefficients between two successive iterations satisfies the following equations:

$$|S_{2B}(k)-S_{2B}(k-1)| \leq 0.02 \quad (15)$$

$$|S_{2F}(k)-S_{2F}(k-1)| \leq 0.02 \quad (16)$$

In practice, convergence was achieved after four iterations. Equations (17) and (18) explain the final input and the output reflection coefficients of the designed IMN and OMN, respectively, which are derived via ESRFT. The IMN and the OMN are constructed by 6 and 5 UEs, respectively. The number of UEs in the IMN and OMN was determined according to the order of the Hurwitz polynomial obtained from the RFT synthesis. Increasing the number of UEs beyond 6 (IMN) and 5 (OMN) did not yield noticeable improvements in TPG or PAE, whereas it led to increased circuit complexity and additional losses.

$$S_{in1}(Z_1) = (17.42\lambda^6 + 81.77\lambda^5 + 11.68\lambda^4 + 48.38\lambda^3 + 48.60\lambda^2 + 49.43\lambda + 17.68)/(17.42\lambda^6-81.77\lambda^5 + 11.68\lambda^4-48.38\lambda^3 + 48.60\lambda^2-49.43\lambda + 17.68) \quad (17)$$

$$S_{out1}(Z_1) = (27.03\lambda^5 + 84.30\lambda^4 + 57.39\lambda^3 + 15.03\lambda^2 + 12.46\lambda + 12.58)/(27.03\lambda^5-84.30\lambda^4 + 57.39\lambda^3-15.03\lambda^2 + 12.46\lambda + 12.58) \quad (18)$$

The non-linear S_{22} obtained from load-pull simulations was kept fixed throughout the ESRFT iterations. However, the reflection coefficients seen by the MNs were updated dynamically in each iteration. ESRFT is particularly applicable to microwave PAs where the active device exhibits noticeable feedback effects (non-negligible S_{12}), typically at frequencies above 1GHz, and to high-power devices with significant parasitic elements. For nearly unilateral devices, ESRFT reduces to the conventional SRFT. Prior device stabilization is required before applying ESRFT.

Fig. 10 shows the flowchart of the ESRFT design procedure used in this work, including device characterization, SRFT-based synthesis, Richard extraction, iterative reflection coefficient updates, and performance-based convergence checking.

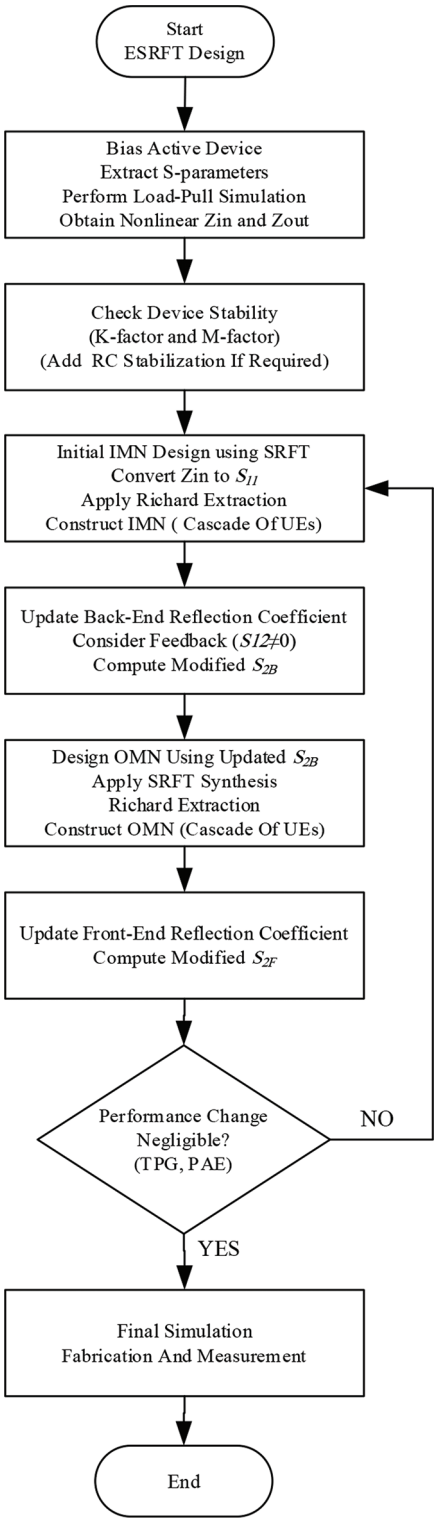

Fig. 10. Design flow of the proposed enhanced simple real frequency technique-based power amplifier.

VII. Results

Fig. 11a shows the simulation and measurement results of the TPG and the PAE of the PA using the designed MNs. It is shown that the PA has a gain up to 13 dB and a PAE up to 70% in a wide frequency band between 0.8 GHz and 1.6 GHz for an input power of 16 dBm, and Fig. 11b shows the simulation and measurement results of the third and the fundamental harmonics in a wide frequency range. It is seen that the third harmonic has been suppressed at least up to 25 dBc.

Fig. 12a shows the S_{11} and S_{22} parameters of the basic PA and the proposed PA versus frequency sweep with an input power of 16 dBm, and Fig. 12b shows the TPG

http://dx.doi.org/10.14500/aro.12657

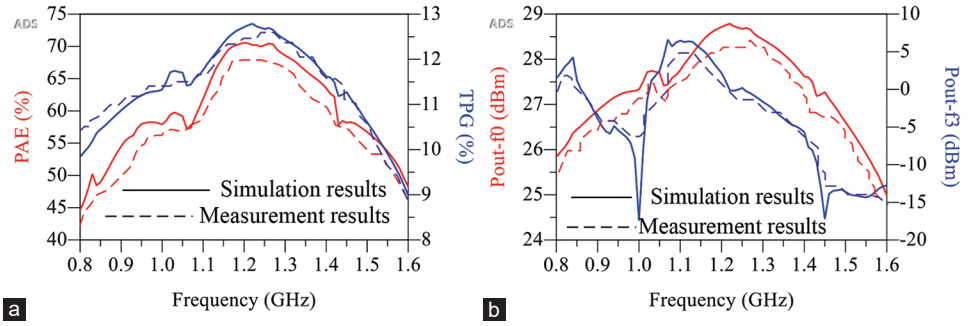

Fig. 11. Simulation and measurement results of the proposed power amplifier (PA): (a) Gain and power added efficiency of the proposed PA, (b) fundamental and third harmonic of the proposed PA for input power of 16 dBm.

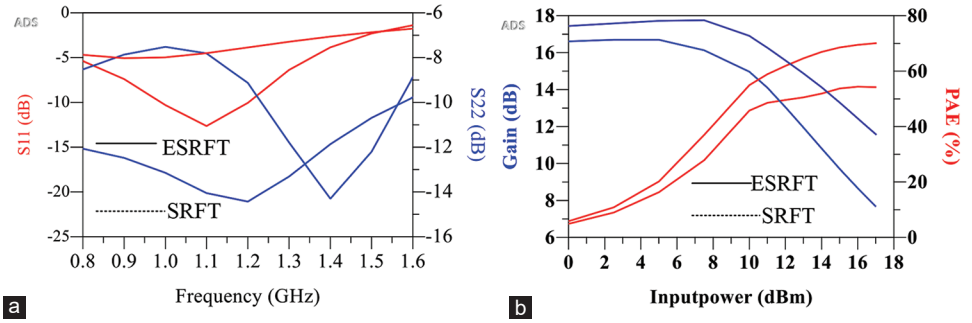

Fig. 12. Basic power amplifier (PA) and the proposed PA: (a) S_{11} and S_{22} parameters versus frequency sweep with an input power of 16 dBm, (b) Transducer power gain and power added efficiency versus input power sweep at operating frequency of 1.3 GHz.

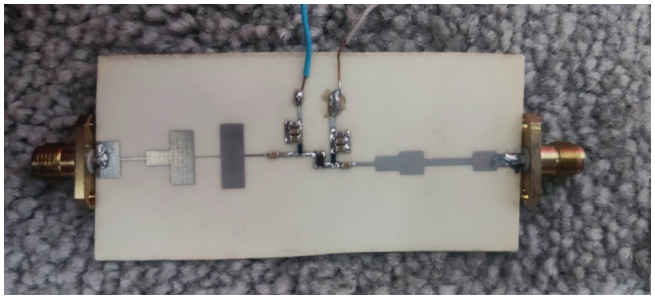

Fig. 13. The proposed power amplifier prototype.

TABLE I
COMPARISON TABLE FOR PROPOSED PA AND OTHER WORKS

References	Bandwidth (GHZ%)	Gain (dB)	PAE (%)	Pout (dBm)
Golestanifar and Karimi, 2021	2.3–2.5 (8)	10–12	35–55	27
Ekhteraei, Hayati and Shama, 2019	2.3–2.5 (8)	10	35–76	26
Hayati, Zarghami and Grebennikov, 2022	2–2.6 (26)	12	30–80	24
Hayati and Shama, 2017	1.75–1.85 (6)	10	76	23
Duan, et al., 2024	1–1.8 (57)	10.7	50–64	26
Proposed PA	0.8–1.6 (66)	9–13	45–70	28

Pout(dBm), PAE: Power added efficiency, PA: Power amplifier

and the PAE versus input power sweep at the operating frequency of 1.3 GHz. According to Fig. 11a, there is a good modification for S_{11} and S_{22} parameters, which shows that the matching has been improved at the input and the output ports for the proposed PA or ESRFT compared to the basic PA or SRFT. Furthermore, considering Fig. 12b, the PAE and the TPG of the proposed PA surpass those of the basic PA. Therefore, it is comprehended that the ESRFT outperforms the SRFT.

Fig. 13 shows the proposed PA prototype. All simulations were carried out using ADS 2020. To obtain accurate simulation results, a high-level non-linear and high-frequency Statz model of the transistor ATF-34143 Ga-As FET with a Q-point of IDS=300 mA, and VDS=3 V, has been utilized. The microstrip substrate is Rogers 4003 with a thickness of 31 mil.

Finally, to compare the designed PA with other works, a comparison table describes some features and characteristics of the proposed PA and the other works in Table I. To have a fair comparison, only papers that have used the same transistor are applied here. It is seen that the proposed PA has a wide bandwidth from 0.8 GHz to 1.6 GHz.

VIII. CONCLUSION

In this paper, a wide-band microstrip PA was designed using the proposed ESRFT. Unlike conventional SRFT, which treats IMN and OMN as two independent single-matching problems under a quasi-unilateral assumption, ESRFT reformulates the synthesis as a coupled double-matching problem under bilateral device conditions. By iteratively updating front-end and back-end reflection coefficients, ESRFT accounts for parasitic feedback effects and improves the overall matching performance. Compared to conventional SRFT, ESRFT requires four redesign iterations and approximately 35% higher computational effort. However, it achieved about 16% improvement in maximum PAE and better wide-band

matching characteristics. The fabricated PA demonstrates operation from 0.8 GHz to 1.6 GHz with up to 70% PAE and improved harmonic suppression. ESRFT requires prior device stabilization and is most beneficial for microwave PAs where feedback effects are non-negligible. For nearly unilateral devices, the method converges to conventional SRFT behavior. Future research may extend ESRFT to multi-band and Doherty architectures, integrate non-linear model updating within the iterative loop, and investigate automated convergence acceleration techniques.

REFERENCES

Carlin, H., 1977. A new approach to gain-bandwidth problems. *IEEE Transactions on Circuits and Systems,* 24**,** pp.170-175.

Duan, Y.W., Xu, J., Su, J.H., Zhao, M., Liu, F., and Zhou, G.Q., 2024. Low-voltage continuous class-F wideband power amplifier. *IEEE Microwave and Wireless Technology Letters,* 34**,** pp.639-642.

Ekhteraei, M., Hayati, M., and Shama, F., 2019. High-efficiency low voltage inverse class-F power amplifier design based on harmonic control network analysis. *IEEE Transactions on Circuits and Systems I: Regular Papers,* 67**,** pp.806-814.

Golestanifar, A., and Karimi, G., 2021. RF power amplifier design using microstrip ring resonator based on image parameter method. *International Journal of Circuit Theory and Applications,* 49**,** pp.2074-2081.

Hayati, M., and Shama, F., 2017. A high-efficiency narrow-band class-F power amplifier integrated with a microstrip suppressing cell. *Analog Integrated Circuits and Signal Processing,* 90**,** pp.351-359.

Hayati, M., Zarghami, S., and Grebennikov, A., 2022. Design of a compact 2.4 GHz class-F power amplifier with high power added efficiency. *IETE Journal of Research,* 68**,** pp.1243-1250.

Jia, P., You, F., He, S., and Qian, X., 2018. A 0.25-1.25-GHz high-efficiency power amplifier with computer-aided design based on optimized impedance solution continuum. *IEEE Microwave and Wireless Components Letters,* 28**,** pp.443-445.

Kouhalvandi, L., Ceylan, O., and Ozoguz, S., 2020. Automated deep neural learning-based optimization for high performance high power amplifier designs. *IEEE Transactions on Circuits and Systems I: Regular Papers,* 67**,** pp.4420-4433.

Krauss, H.L., Bostian, C.W., and Raab, F.H., 1991. *Solid State Radio Engineering*. John Wiley & Sons, United States.

Mohamadpour, G., Karimi, S., and Roshani, S., 2025. Dual-band power divider with wide suppression band: Artificial intelligence modeling for performance confirmation. *Aro-the Scientific Journal of Koya University,* 13**,** pp.27-33.

Roshani, S., Yahya, S.I., Khazaei, S., Roshani, S., and Karami, B., 2024. Design and fabrication of a microstrip low-pass filter with a wide stopband using a windmill-shaped resonator. *Aro-the Scientific Journal of Koya University,* 12**,** pp.201-208.

Roshani, S., Yahya, S.I., Najafi, B., Jadidian, A., Karimi, M., and Roshani, S., 2025. Optimizing a compact ring coupler with neural network modeling for enhanced performance in radio frequency applications. *Aro-the Scientific Journal of Koya University,* 13**,** pp.122-130.

Tran, K., Henderson, R., and Gengler, J., 2019. Design of a 1-2.8-GHz 100-W power amplifier with bounded performance technique. *IEEE Transactions on Microwave Theory and Techniques,* 67**,** pp.3707-3715.

Yang, Z., Yao, Y., Liu, Z., Li, M., Li, T., and Dai, Z., 2018. Design of high efficiency broadband continuous class-F power amplifier using real frequency technique with finite transmission zero. *IEEE Access,* 6**,** pp.61983-61993.

Yarman, B.S., 2008. *Design of Ultra Wideband Antenna Matching Networks: Via Simplified Real Frequency Technique*. Springer, Berlin.

Yarman, B.S., 2010. *Design of Ultra Wideband Power Transfer Networks*. John Wiley and Sons, United States.

Youla, D., 1964. A new theory of broad-band matching. *IEEE Transactions on Circuit Theory,* 11**,** pp.30-50.